

# New Eigensystem Realization Algorithm for Dynamic Systems with Multiple Inputs

Taehyoun Kim

Boeing Commercial Airplane Group  
P.O. Box 3707, MS 03-KR  
Seattle, Washington 98124-2207

## Abstract

Presented in this paper is a new, efficient discrete-time domain system identification and model reduction method for large-scaled linear dynamic systems with multiple inputs. The method is based on a modification of the classical Eigensystem Realization Algorithm (ERA) and a simultaneous injection of multiple inputs, so called the Single-Composite-Input (SCI). Since the system response is sampled almost exclusively for the single representative input instead of the multiple individual inputs, this technique can significantly reduce the model construction time as well as the amount of the sampled data. For derivation of the new algorithm, a singular value decomposition is performed using a single set of output measurements that are not necessarily attributed to pulse inputs. Application to general computational fluid dynamic systems and formulation of reduced-order aeroelastic models are also presented. Aerodynamic and aeroelastic systems modeled by the vortex lattice and CFL3D code are presented for a demonstration of the method. Based on the reduced computation time and excellent results obtained from the reduced-order models, the proposed algorithm shows a great potential as a linear system identification and model reduction tool for large-scaled systems subjected to multiple inputs.

## Nomenclature

$\mathbf{A} \mathbf{B} \mathbf{C} \mathbf{D}$	System matrices
$\mathbf{A}_{d1} \mathbf{A}_{d2}$	Aeroelastic system matrices

$\mathbf{A}_s \mathbf{B}_s \mathbf{C}_s$	Structural system matrices
$b$	Reference length
$C_{ij}$	Cross-correlation coefficient
$E$	Expected value
$\mathbf{K}$	Covariance matrix defined in (48)
$L$	Dimension of original system
$M$	Number of time or frequency samples or Mach number
$\mathbf{m} \mathbf{c} \mathbf{k}$	Mass, damping, stiffness matrices
$\mathbf{p}$	$(R_1 \times 1)$ generalized coordinate vector
$q$	Dynamic pressure ( $\equiv \frac{1}{2} \rho V^2$ )
$R$	Number of chosen singular modes or the dimension of realized model
$R_1$	Number of chosen KL modes
$s$	Laplace variable
$t$	Real time
$\mathbf{u}$	$(N_i \times 1)$ input or generalized structural coordinate vector
$u_i$	$i$ -th input or structural coordinate
$V$	Air speed
$\mathbf{x}$	$(L \times 1)$ state or aerodynamic state vector
$\mathcal{X}$	Fourier transform of $\mathbf{x}$
$\mathbf{y}$	$(N_o \times 1)$ output vector or $(N_i \times 1)$ generalized aerodynamic force vector
$\mathbf{y}_i^n$	Pulse response due to $i - th$ input
$\phi_i$	KL mode
$\Phi$	KL modal matrix
$\rho$	Air density

$\tau$	Reduced time ( $\equiv \frac{Vt}{b}$ )
$\omega$	Frequency (rad/sec)
$\omega_c$	Maximum cut-off frequency

### *Subscripts*

$i$	Input
$o$	Output
$R$	Reduced
$ref$	Reference
$s$	Structure

## 1 Introduction

Most modern dynamic models are constructed based on finite spatial discretizations of continuous systems, often resulting in a considerable number of degrees of freedom in the model. Consequently, for fast and efficient estimation of dynamic behavior as well as optimizations and closed-loop control designs, a model reduction must be accompanied. Essential requirements for reduced-order dynamic model are that the size of the system must not be too large, the model must be robust and have a good fidelity, it must be in the state-space, time domain formulation for implementation of active control systems and nonlinear time analysis, and finally, the reduction process itself must not be too expensive.

There have been many model reduction methods available, but most of them require modifying the main frame of the computational model, and are prone to a long model construction time if the model is subjected to many driving inputs. The latter in particular is true in unsteady Computational Fluid Dynamic (CFD) applications where the moving solid boundary is often described by many structural

mode inputs. For example, a typical Boeing commercial airplane is modeled by as many as 200 structural modes.

Recently, the Eigensystem Realization Algorithm (ERA)[1] was used successfully in application of CFL3D for aeroelastic flutter predictions [2],[3]. This method, which is usually used as a system identification technique, has a very attractive feature in that unlike model reduction methods based on Galerkin scheme[4] there is no need for on-line implementation of the algorithm. That is, it is a post-processing tool that identifies and generates system matrices based on the input and output data alone. Unfortunately, if the unsteady CFD model is driven by multiple structural inputs the computation time required to obtain all the pulse responses increases proportional to the number of the inputs, making the ERA slow and inefficient.

Kim et al [5],[6] introduced the concept of the Single-Composite-Input (SCI) in applications of Karhunen-Loeve method to unsteady CFD models in time and frequency domains. The idea herein was that for a linear system, one can apply the multiple inputs simultaneously and get all the system responses that are necessary for the model reduction. Since the computational model needed to be executed only for the representative input, the model construction time was significantly reduced. In this paper, the same approach is adopted for fast and efficient model reduction of linear, finite-dimensional, discrete-time systems. To accommodate the SCI within the framework of ERA, it is necessary to modify the original algorithm. In particular, it will be shown that the new formulation does not rely on the system Markov parameters explicitly. Instead, it performs the singular-value-decomposition (SVD) directly on the output measurements that are in general not attributed to pulse inputs. Statistically independent random numbers are used in lieu of the pulses for the multiple input signals. Naturally, the new algorithm can also be used towards system identification provided that all the time measurements are available from experiments. Application of the SCI/ERA to computational fluid dynamic systems and formulation of reduced-order aeroelastic models are also presented. It is shown that

depending on how the displacement and velocity inputs on the moving boundary are treated, two different kinds of reduced-order aerodynamic and aeroelastic models could be generated.

For a demonstration of the proposed method, two CFD models are considered. They are the Vortex Lattice Model (VLM) for inviscid, subsonic, incompressible flow, and the CFL3D for viscous, transonic, compressible flow. Reduced-order aeroelastic models are also constructed by combining the reduced aerodynamic models and the structural system. It is shown that not only the new method shortens the model construction time substantially, but the accuracy of the resulting reduced-order models is excellent. The proposed scheme has a great potential as a linear system identification and model reduction tool for large-scaled systems subjected to multiple inputs.

## 2 Review of Pulse/ERA

In this section, the Pulse/ERA (also known as ERA) is reviewed. For simplicity, only its fundamental state-space realization theory which is attributed to Ho and Kalman[7] is discussed. For a general description of the method, see Ref.[8]. It is assumed that the system under consideration can be described in the following finite-dimensional, discrete-time form:

$$\mathbf{x}^{n+1} = \mathbf{A} \mathbf{x}^n + \mathbf{B} \mathbf{u}^n \quad (1)$$

$$\mathbf{y}^n = \mathbf{C} \mathbf{x}^n + \mathbf{D} \mathbf{u}^n \quad (2)$$

where

$$\mathbf{x} \equiv (L \times 1) \text{ state vector} \quad (3)$$

$$\mathbf{u} \equiv (N_i \times 1) \text{ input vector} \quad (4)$$

$$\mathbf{y} \equiv (N_o \times 1) \text{ output vector} \quad (5)$$

The system matrices  $(\mathbf{A}, \mathbf{B})$ ,  $(\mathbf{A}, \mathbf{C})$  are assumed controllable and observable. First, given  $M + 1$  equally distributed time steps,  $t^n \equiv n \Delta t$  ( $n = 0, 1, 2, \dots, M$ ), for a

single  $i$ -th input vector the system output is sampled subjected to the unit pulse,

$$u_i^n = \delta^n \equiv \begin{cases} 1 & (n = 0) \\ 0 & (n = 1, 2, \dots, M) \end{cases} \quad (6)$$

Assuming zero initial condition,  $\mathbf{x}^0 \equiv \mathbf{x}(0) = \mathbf{0}$ , one obtains

$$\begin{aligned} \mathbf{y}_i^0 &= \mathbf{d}_i \\ \mathbf{y}_i^1 &= \mathbf{C} \mathbf{b}_i \\ \mathbf{y}_i^2 &= \mathbf{C} \mathbf{A} \mathbf{b}_i \\ \mathbf{y}_i^3 &= \mathbf{C} \mathbf{A}^2 \mathbf{b}_i \\ &\vdots \\ \mathbf{y}_i^M &= \mathbf{C} \mathbf{A}^{M-1} \mathbf{b}_i \end{aligned} \quad (7)$$

where

$$\mathbf{b}_i \equiv \text{i-th column of } \mathbf{B} \quad (8)$$

$$\mathbf{d}_i \equiv \text{i-th column of } \mathbf{D} \quad (9)$$

The constant matrices in the above sequence are known as the Markov parameters[1].

This step is repeated  $N_i$  times for all inputs creating the sequence of pulse-response matrices:

$$\mathbf{Y}^n \equiv [\mathbf{y}_1^n \ \mathbf{y}_2^n \ \dots \ \mathbf{y}_{N_i}^n] \ (n = 0, 1, 2, \dots, M) \quad (10)$$

Next, based on the system Markov parameters define  $N_o \times (N_i \times (M - 1))$  Hankel matrices:

$$\begin{aligned} \mathbf{H}_0 &\equiv [\mathbf{Y}^1 \ \mathbf{Y}^2 \ \dots \ \mathbf{Y}^{M-1}] \\ &= \mathbf{C} [\mathbf{I} \ \mathbf{A} \ \mathbf{A}^2 \ \dots \ \mathbf{A}^{M-2}] \mathbf{B} \end{aligned} \quad (11)$$

$$\begin{aligned} \mathbf{H}_1 &\equiv [\mathbf{Y}^2 \ \mathbf{Y}^3 \ \dots \ \mathbf{Y}^M] \\ &= \mathbf{C} [\mathbf{A} \ \mathbf{A}^2 \ \dots \ \mathbf{A}^{M-1}] \mathbf{B} \end{aligned} \quad (12)$$

SVD of  $\mathbf{H}_0$  yields

$$\begin{aligned}\mathbf{H}_0 &\equiv \mathbf{U} \mathbf{\Sigma} \mathbf{V}^T \\ &\simeq [\mathbf{U}_R \ \mathbf{U}_D] \begin{bmatrix} \mathbf{\Sigma}_R & \mathbf{0} \\ \mathbf{0} & \mathbf{0} \end{bmatrix} \begin{bmatrix} \mathbf{V}_R^T \\ \mathbf{V}_D^T \end{bmatrix} \\ &= \mathbf{U}_R \mathbf{\Sigma}_R^{1/2} \mathbf{\Sigma}_R^{1/2} \mathbf{V}_R^T\end{aligned}\quad (13)$$

where  $R \equiv \text{rank}(\mathbf{H}_0)$ . Finally, a *balanced* realization of the system under question is obtained by pseudo-inverting various submatrix components as

$$\mathbf{D} = \mathbf{Y}^0 \quad (N_o \times 1) \quad (14)$$

$$\mathbf{C} \simeq \mathbf{U}_R \mathbf{\Sigma}_R^{1/2} \quad (N_o \times R) \quad (15)$$

$$\mathbf{B} \simeq \text{the first } N_i \text{ columns of } \mathbf{\Sigma}_R^{1/2} \mathbf{V}_R^T \quad (R \times N_i) \quad (16)$$

$$\mathbf{A} \simeq \mathbf{\Sigma}_R^{-1/2} \mathbf{U}_R^T \mathbf{H}_1 \mathbf{V}_R \mathbf{\Sigma}_R^{-1/2} \quad (R \times R) \quad (17)$$

Since  $R \ll L$ , the above model represents a reduced-order realization of the original system. Note that the realization is optimal in that it is balanced between *inputs* and *outputs*. However, the total number of samples taken is  $N_i \times (M+1)$ , which increases proportional to the number of inputs. Also, for an accurate system identification  $\mathbf{H}_0$  must have sufficient columns and rows, i.e.,  $N_i \times (M-1) \geq R$  and  $N_o \geq R$ . Figure 1 shows a schematic of the Pulse/ERA procedure.

For a very large data set  $\mathbf{Y}^n$  with many time steps and a large number of inputs, the Eigensystem Realization Algorithm/Data Correlations (ERA/DC) method is preferred to compress the amount of data and reduce the computation time required for the SVD of the Hankel matrix. See Ref.[1] for details.

### 3 SCI/ERA

The new method proceeds as follows. First, individual pulse responses are sampled for the first two time steps:

$$\mathbf{Y}^0 = [\mathbf{y}_1^0 \ \mathbf{y}_2^0 \ \dots \ \mathbf{y}_{N_i}^0] \quad (18)$$

$$\mathbf{Y}^1 = [\mathbf{y}_1^1 \ \mathbf{y}_2^1 \ \dots \ \mathbf{y}_{N_i}^1] \quad (19)$$

Next, construct the SCI as

$$\mathbf{b}_{SCI}^n \equiv \sum_{i=1}^{N_i} \mathbf{b}_i r_i^n \quad (\text{for states}) \quad (20)$$

$$\mathbf{d}_{SCI}^n \equiv \sum_{i=1}^{N_i} \mathbf{d}_i r_i^n \quad (\text{for outputs}) \quad (21)$$

where

$$r_i^n \equiv \text{a sequence of arbitrary numbers} \quad (22)$$

To ensure independency of the inputs, the signals must be as uncorrelated as possible.

In an ideal case they would be statistically uncorrelated random signals, i.e.,  $C_{ij}(m) = E[r_i^n r_j^{n-m}] = 0$  for  $i \neq j$ , but they are hard to construct for numerical analysis.

Subject to the SCI, we sample the system response  $\mathbf{y}^n$  for  $n = 0, 1, 2, \dots, M$ , and get

$$\begin{aligned} \mathbf{y}_{c0}^n &\equiv \mathbf{C} \mathbf{x}^n \\ &= \mathbf{y}^n - \sum_{i=1}^{N_i} \mathbf{y}_i^0 r_i^n \end{aligned} \quad (23)$$

$$\begin{aligned} \mathbf{y}_{c1}^n &\equiv \mathbf{C} \mathbf{A} \mathbf{x}^n \\ &= \mathbf{y}^{n+1} - \sum_{i=1}^{N_i} \mathbf{y}_i^0 r_i^{n+1} - \sum_{i=1}^{N_i} \mathbf{y}_i^1 r_i^n \end{aligned} \quad (24)$$

Note that  $\mathbf{y}_{c0}^n, \mathbf{y}_{c1}^n$  are measurements of the states in the reduced dimension of  $\mathbf{C}$  and  $\mathbf{C} \mathbf{A}$ . Similar to the Hankel matrices, define

$$\begin{aligned} \mathbf{H}_{c0} &\equiv [\mathbf{y}_{c0}^1 \ \mathbf{y}_{c0}^2 \ \dots \ \mathbf{y}_{c0}^{M-1}] \\ &= \mathbf{C} [\mathbf{x}^1 \ \mathbf{x}^2 \ \dots \ \mathbf{x}^{M-1}] \end{aligned} \quad (25)$$

$$\begin{aligned} \mathbf{H}_{c1} &\equiv [\mathbf{y}_{c1}^1 \ \mathbf{y}_{c1}^2 \ \dots \ \mathbf{y}_{c1}^{M-1}] \\ &= \mathbf{C} \mathbf{A} [\mathbf{x}^1 \ \mathbf{x}^2 \ \dots \ \mathbf{x}^{M-1}] \end{aligned} \quad (26)$$

SVD of  $\mathbf{H}_{c0}$  yields

$$\begin{aligned} \mathbf{H}_{c0} &\equiv \mathbf{U} \mathbf{\Sigma} \mathbf{V}^T \\ &\simeq [\mathbf{U}_R \ \mathbf{U}_D] \begin{bmatrix} \mathbf{\Sigma}_R & \mathbf{0} \\ \mathbf{0} & \mathbf{0} \end{bmatrix} \begin{bmatrix} \mathbf{V}_R^T \\ \mathbf{V}_D^T \end{bmatrix} \\ &= \mathbf{U}_R \mathbf{\Sigma}_R^{1/2} \mathbf{\Sigma}_R^{1/2} \mathbf{V}_R^T \end{aligned} \quad (27)$$

Once again,  $R \equiv \text{rank}(\mathbf{H}_{c0})$ . The size of the above matrices is  $N_o \times (M - 1)$ ,  $N_i$  times smaller than the previous  $\mathbf{H}_0, \mathbf{H}_1$ . The new realization is then

$$\mathbf{D} = \mathbf{Y}^0 \quad (28)$$

$$\mathbf{C} \simeq \mathbf{U}_R \Sigma_R^{1/2} \quad (29)$$

$$\mathbf{B} \simeq \Sigma_R^{-1/2} \mathbf{U}_R^T \mathbf{Y}^1 \quad (30)$$

$$\mathbf{A} \simeq \Sigma_R^{-1/2} \mathbf{U}_R^T \mathbf{H}_{c1} \mathbf{V}_R \Sigma_R^{-1/2} \quad (31)$$

Unlike the Pulse/ERA, the SCI/ERA is optimal in that it is balanced between *states* and *outputs*. As in the previous method, for an accurate realization  $\mathbf{H}_{c0}$  must have  $(M - 1) \geq R$  and  $N_o \geq R$ . However, the total no. of samples taken is only  $M + 1 + 2 \times N_i$  which is much less than the previous  $N_i \times (M + 1)$  when  $M$  samples of pulse response are taken for each input. Figure 2 shows a schematic of the SCI/ERA procedure.

Two comments regarding the new algorithm are in order. First and foremost, compared to the Pulse/ERA the new algorithm requires a much smaller set of time measurements reducing significantly both the computation time and the bulk of the output data. Second, the new  $\mathbf{H}_{c0}, \mathbf{H}_{c1}$  are constructed based on the sampled system states subjected to combined random inputs, and as such they are not directly related to the Markov parameters. However, the scheme does require the first two pulse responses  $\mathbf{y}_i^0$  and  $\mathbf{y}_i^1$  for each input in order to estimate the state measurements according to Eqs. (23), (24).

Although random signals are used exclusively in this paper, other types of signals can also be used for the SCI provided that they are statistically independent. It is well known that for a linear system any arbitrary response contains the fundamental characteristics under the assumption that the system is controllable and observable. It is this observation, along with the principle of superposition, that the present system identification scheme is based on.

## 4 Alternative Scheme to Increase Measurements

One of the requirements in the ERA methods is that for an accurate model construction one must have a sufficient number of output measurements, more than the number of singular modes that are extractable from the Hankel matrices. Failure to satisfy this requirement implies that we don't have enough modes to approximate the system response. When the requirement is not met, assuming again that  $(\mathbf{A}, \mathbf{C})$  is observable we can expand the data matrices by sampling additional responses as follows.

$$\begin{aligned}
 \mathbf{H}_{c01} &\equiv \begin{bmatrix} \mathbf{C} \\ \mathbf{C}\mathbf{A} \\ \mathbf{C}\mathbf{A}^2 \\ \vdots \\ \mathbf{C}\mathbf{A}^K \end{bmatrix} [\mathbf{x}^1 \ \mathbf{x}^2 \ \dots \ \mathbf{x}^{M-1}] \\
 &= \begin{bmatrix} \mathbf{y}_{c0}^1 & \mathbf{y}_{c0}^2 & \dots & \mathbf{y}_{c0}^{M-1} \\ \mathbf{y}_{c1}^1 & \mathbf{y}_{c1}^2 & \dots & \mathbf{y}_{c1}^{M-1} \\ \dots & \dots & \dots & \dots \\ \mathbf{y}_{cK}^1 & \mathbf{y}_{cK}^2 & \dots & \mathbf{y}_{cK}^{M-1} \end{bmatrix} \quad (32)
 \end{aligned}$$

$$\begin{aligned}
 \mathbf{H}_{c11} &\equiv \begin{bmatrix} \mathbf{C} \\ \mathbf{C}\mathbf{A} \\ \mathbf{C}\mathbf{A}^2 \\ \vdots \\ \mathbf{C}\mathbf{A}^K \end{bmatrix} \mathbf{A} [\mathbf{x}^1 \ \mathbf{x}^2 \ \dots \ \mathbf{x}^{M-1}] \\
 &= \begin{bmatrix} \mathbf{y}_{c1}^1 & \mathbf{y}_{c1}^2 & \dots & \mathbf{y}_{c1}^{M-1} \\ \mathbf{y}_{c2}^1 & \mathbf{y}_{c2}^2 & \dots & \mathbf{y}_{c2}^{M-1} \\ \dots & \dots & \dots & \dots \\ \mathbf{y}_{cK+1}^1 & \mathbf{y}_{cK+1}^2 & \dots & \mathbf{y}_{cK+1}^{M-1} \end{bmatrix} \quad (33)
 \end{aligned}$$

where

$$\begin{aligned}
 \mathbf{y}_{ck}^n &\equiv \mathbf{C}\mathbf{A}^k \mathbf{x}^n \\
 &= \mathbf{y}^{n+k} - \sum_{i=1}^{N_i} \mathbf{y}_i^0 r_i^{n+k} - \sum_{i=1}^{N_i} \mathbf{y}_i^1 r_i^{n+k-1} - \\
 &\quad \dots - \sum_{i=1}^{N_i} \mathbf{y}_i^k r_i^n
 \end{aligned}$$

$$= \mathbf{y}^{n+k} - \sum_{j=1}^{k+1} \sum_{i=1}^{N_i} \mathbf{y}_i^{j-1} \mathbf{r}_i^{n+k+1-j} \quad (34)$$

SVD of the new  $\mathbf{H}_{c0}$  leads to

$$\begin{aligned} \mathbf{H}_{c01} &\equiv \mathbf{U}_1 \boldsymbol{\Sigma}_1 \mathbf{V}_1^T \\ &\simeq [\mathbf{U}_{1R} \ \mathbf{U}_{1D}] \begin{bmatrix} \boldsymbol{\Sigma}_{1R} & \mathbf{0} \\ \mathbf{0} & \mathbf{0} \end{bmatrix} \begin{bmatrix} \mathbf{V}_{1R}^T \\ \mathbf{V}_{1D}^T \end{bmatrix} \\ &= \mathbf{U}_{1R} \boldsymbol{\Sigma}_{1R}^{1/2} \boldsymbol{\Sigma}_{1R}^{1/2} \mathbf{V}_{1R}^T \end{aligned} \quad (35)$$

from which we obtain

$$\mathbf{D} = \text{the first } N_o \text{ rows of } \mathbf{Y}_c^0 \quad (36)$$

$$\mathbf{C} \simeq \text{the first } N_o \text{ rows of } \mathbf{U}_{1R} \boldsymbol{\Sigma}_{1R}^{1/2} \quad (37)$$

$$\mathbf{B} \simeq \boldsymbol{\Sigma}_{1R}^{-1/2} \mathbf{U}_{1R}^T \mathbf{Y}_c^1 \quad (38)$$

$$\mathbf{A} \simeq \boldsymbol{\Sigma}_{1R}^{-1/2} \mathbf{U}_{1R}^T \mathbf{H}_{c11} \mathbf{V}_{1R} \boldsymbol{\Sigma}_{1R}^{-1/2} \quad (39)$$

where

$$\mathbf{Y}_c^n \equiv \begin{bmatrix} \mathbf{y}_1^n & \mathbf{y}_2^n & \cdots & \mathbf{y}_{N_i}^n \\ \mathbf{y}_1^{n+1} & \mathbf{y}_2^{n+1} & \cdots & \mathbf{y}_{N_i}^{n+1} \\ \cdots & \cdots & \cdots & \cdots \\ \mathbf{y}_1^{n+K+1} & \mathbf{y}_2^{n+K+1} & \cdots & \mathbf{y}_{N_i}^{n+K+1} \end{bmatrix} \quad (n = 0, 1) \quad (40)$$

The total number of measurements available is now  $(K+1) \times N_o$ . It is noted that the additional time samples are required for the pulse response as well as for the response due to the SCI. More specifically, if  $K$  blocks of outputs are to be added pulse responses due to each input must be sampled at  $K$  additional time steps in addition the first two time steps,  $t = 0$  and  $t = \Delta t$ . Also, the response due to the SCI must be sampled at  $K$  additional steps beyond the  $M$ -th step. The total number of samples to be taken is thus  $M+1+K+(2+K) \times N_i$ .  $K$  must be sufficiently large enough to satisfy the measurement requirement,  $(K+1) \times N_o \geq R$ . Needless to say, this scheme requires extra computation time because of the additional time samples required in the data set.

## 5 Time Signals for Simultaneous Excitation

A few candidate signals for the SCI are introduced in this section. Note that for an ideal linear model any of these SCIs can be used and all of them should yield ROMs of essentially the same quality.

### 5.1 Random inputs based SCI (RSCI)

It is natural to use random signals for construction of SCI. That is, use

$$r_i^n \equiv \text{a sequence of random numbers} \quad (41)$$

in Eqs. (20) and (21).

### 5.2 Filtered inputs based SCI (FSCI)

To inject smooth inputs, one can filter the random signals through a low-pass filter. That is,

$$\begin{aligned} r_i^n &= r_{fi}^n \\ &\equiv \text{a sequence of filtered random numbers} \end{aligned} \quad (42)$$

Using the low frequency signals will allow better convergence when applying the SCI to CFD models. Furthermore, since the frequency content is limited it is possible to generate a smaller ROM directly from the SCI/ERA without any further reduction. A potential drawback is that if the filtered signals become too narrowly banded, they may not be as uncorrelated as desired. However, based on the theory of ergodicity [9], the statistical independence could be fortified by using longer signals and sampling the response for a longer period of time.

### 5.3 Step inputs based SCI (SSCI)

In analogy to a single step input, one can apply multiple step inputs in a sequential manner:

$$r_i^n = u_i^{n-k_i}$$

$$\equiv \text{a step input applied at } k_i\text{-th step} \quad (43)$$

where

$$u_i^{n-k_i} \equiv \begin{cases} 0 & (n = 1, 2, \dots, k_i - 1) \\ 1 & (n \geq k_i) \end{cases} \quad (44)$$

To assure independence of the inputs, the onsets of the signals must be apart from each other by a sufficient number of steps, i.e.,  $k_i$  must be large enough.

## 5.4 Pulse inputs based SCI (PSCI)

One can also apply multiple pulse inputs in a sequential manner:

$$\begin{aligned} r_i^n &= \delta_i^{n-k_i} \\ &\equiv \text{a step input applied at } k_i\text{-th step} \end{aligned} \quad (45)$$

where

$$\delta_i^{n-k_i} \equiv \begin{cases} 1 & (n = k_i) \\ 0 & (n = \text{all other points}) \end{cases} \quad (46)$$

Again,  $k_i$  must be large enough to ensure independency of the applied signals.

## 6 Second Reduction Based On FDKL/SCI Method

In applications of discrete-time computational models, there exist two conflicting requirements for the incremental time step  $\Delta t$ . For numerical convergence one has to adopt a sufficiently small  $\Delta t_1$ . On the other hand, given the highest frequency of interest,  $\omega_c$ , Nyquist criterion requires  $\Delta t_2 \leq \frac{\pi}{\omega_c}$ . Usually, for practical purposes  $\Delta t_2 \gg \Delta t_1$ . For instance, in a structural model that is coupled with a CFD model for aeroelastic applications, the highest mode usually has a much lower natural frequency than the highest frequency content in the aerodynamic model. If the signals used in the ERA methods are sharp as in the random, step, or pulse inputs, the SCI will excite all the system dynamics and hence this characteristic will be carried

over to the ERA based reduced-order model. As a result, the ERA reduced-order model (ROM) is prone to have a large dimension to span the same high frequency range as the original full-order model (FOM), which suggests that there may be a room for further order reduction in the ROM. To perform a second order reduction, one can apply the Frequency-Domain Karhunen-Loeve (FDKL) method to the ERA ROM defined by matrices, (28)-(31), wherein frequency samples of the system within the given frequency range,  $(-\omega_c, \omega_c)$  are used to extract optimal modes, and a new reduced-order model is constructed via the Galerkin's approximation[10]. According to the method, the optimal or so called KL modes  $\phi_i$  are the eigenmodes of the covariance matrix  $\mathbf{K}$ :

$$\mathbf{K} \phi_i = \lambda_i \phi_i \quad (47)$$

where

$$K_{ij} \equiv \mathcal{X}(\omega_i) \mathcal{X}(\omega_j)^{*T} \quad (48)$$

$$\begin{aligned} \omega_i &\equiv \text{sampling frequencies} \\ &= [\omega_1 \ \omega_2 \ \dots \ \omega_M] \end{aligned} \quad (49)$$

where  $\omega_1 = -\omega_c$  and  $\omega_M = \omega_c$ .  $\mathcal{X}_i(\omega_i)$  are the frequency solutions of the ERA ROM subjected to the single-composite-input described by (20) and (21) except that it is prescribed in the frequency domain. Once the optimal modes are obtained, assume

$$\mathbf{x} \simeq \Phi \mathbf{p} \quad (50)$$

where

$$\Phi \equiv [\phi_1 \ \phi_2 \ \dots \ \phi_{R_1}] \quad (51)$$

$$\mathbf{p} \equiv \left\{ \begin{array}{c} p_1 \\ p_2 \\ \vdots \\ p_{R_1} \end{array} \right\} \quad (52)$$

$R_1$  is set to be equal to the rank of the covariance matrix which is usually smaller than  $R$ . After inserting (50) into (1) and (2) with the ERA ROM matrices, premultiplying both sides by  $\Phi^T$  yields a new reduced-order model as

$$\mathbf{p}^{n+1} = \mathbf{A}_1 \mathbf{p}^n + \mathbf{B}_1 \mathbf{u}^n \quad (53)$$

$$\mathbf{y}^n = \mathbf{C}_1 \mathbf{p}^n + \mathbf{D} \mathbf{u}^n \quad (54)$$

where

$$\mathbf{A}_1 \equiv \Phi^T \mathbf{A} \Phi \quad (55)$$

$$\mathbf{B}_1 \equiv \Phi^T \mathbf{B} \quad (56)$$

$$\mathbf{C}_1 \equiv \mathbf{C} \Phi \quad (57)$$

The dimension of the new model is  $(R_1 \times R_1)$ .

## 7 Application to CFD Model

In this section, application of the proposed model reduction/system identification method to large-scaled CFD models is discussed. Unlike the general system described by Eq. (1) and (2), an unsteady fluid dynamic system is driven by displacement and velocity of its moving boundary surface simultaneously as they both contribute to the normal downwash on the surface. If one considers a statically nonlinear, dynamically linearized flow field, the unsteady fluid motion can be described as

$$\mathbf{x}^{n+1} = \mathbf{A} \mathbf{x}^n + \mathbf{B}_0 \mathbf{u}^n + \mathbf{B}_1 \dot{\mathbf{u}}^n \quad (58)$$

$$\mathbf{y}^n = \mathbf{q} (\mathbf{C} \mathbf{x}^n + \mathbf{D}_0 \mathbf{u}^n + \mathbf{D}_1 \dot{\mathbf{u}}^n) \quad (59)$$

where

$$\mathbf{x} \equiv (L \times 1) \text{ fluid states} \quad (60)$$

$$\mathbf{u} \equiv (N_i \times 1) \text{ generalized displacements} \quad (61)$$

$$\dot{\mathbf{u}} \equiv (N_i \times 1) \text{ generalized velocities} \quad (62)$$

$$\mathbf{y} \equiv (N_i \times 1) \text{ generalized aerodynamic forces} \quad (63)$$

$$q \equiv \text{dynamic pressure} \quad (64)$$

It is noted that the above equations progress in non-dimensional time,  $\tau \equiv \frac{Vt}{b}$ , rather than in the real time  $t$  and  $(\dot{\phantom{x}})$  is the first derivative with respect to  $\tau$ . In fact, the dependency of the normal downwash on air speed disappears when the equations are discretized in  $\tau$ , as in Eqs. (58) and (59). The structural degrees of freedom,  $u_i$  are the generalized coordinates associated with structural modes. These modes are used to describe the motion of the lifting surface. Two different types of reduced-order fluid dynamic models can be obtained depending on how the inputs are treated. If necessary, the FDKL/SCI can be performed for additional reduction.

## 7.1 Aerodynamic ROM with displacement and velocity inputs

One can treat  $\mathbf{u}^n$  and  $\dot{\mathbf{u}}^n$  separately as independent inputs. Thus, for the pulse inputs

$$u_i^n = \dot{u}_i^n = \delta^n \equiv \begin{cases} 1 & (n=0) \\ 0 & (n=1, 2, \dots, M) \end{cases} \quad (65)$$

for  $i = 1, 2, \dots, N_i$ , we obtain the corresponding responses  $\mathbf{y}_i^0, \mathbf{y}_i^1$  at the first two time steps. Let us define

$$\mathbf{Y}^0 = [\mathbf{y}_1^0 \mathbf{y}_2^0 \dots \mathbf{y}_{N_i}^0 \mathbf{y}_{N_i+1}^0 \mathbf{y}_{N_i+2}^0 \dots \mathbf{y}_{2N_i}^0] \quad (66)$$

$$\mathbf{Y}^1 = [\mathbf{y}_1^1 \mathbf{y}_2^1 \dots \mathbf{y}_{N_i}^1 \mathbf{y}_{N_i+1}^1 \mathbf{y}_{N_i+2}^1 \dots \mathbf{y}_{2N_i}^1] \quad (67)$$

where the first  $N_i$  samples are due to the pulses in  $\mathbf{u}^n$  and the next  $N_i$  ones are due to the pulses in  $\dot{\mathbf{u}}^n$ . Next, we prepare the following inputs,

$$\mathbf{b}_{SCI}^n \equiv \sum_{i=1}^{N_i} \mathbf{b}_{0i} r_i^n + \sum_{i=1}^{N_i} \mathbf{b}_{1i} r_{N_i+i}^n \quad (68)$$

$$\mathbf{d}_{SCI}^n \equiv \sum_{i=1}^{N_i} \mathbf{d}_{0i} r_i^n + \sum_{i=1}^{N_i} \mathbf{d}_{1i} r_{N_i+i}^n \quad (69)$$

Subject to the SCI, we sample the system response  $\mathbf{y}^n$  and get

$$\mathbf{y}_{c0}^n \equiv \mathbf{y}^n - \sum_{i=1}^{2N_i} \mathbf{y}_i^0 r_i^n \quad (70)$$

$$\mathbf{y}_{c1}^n \equiv \mathbf{y}^{n+1} - \sum_{i=1}^{2N_i} \mathbf{y}_i^0 r_i^{n+1} - \sum_{i=1}^{2N_i} \mathbf{y}_i^1 r_i^n \quad (71)$$

Define

$$\mathbf{H}_{c0} \equiv [\mathbf{y}_{c0}^1 \ \mathbf{y}_{c0}^2 \ \dots \ \mathbf{y}_{c0}^{M-1}] \quad (72)$$

$$\mathbf{H}_{c1} \equiv [\mathbf{y}_{c1}^1 \ \mathbf{y}_{c1}^2 \ \dots \ \mathbf{y}_{c1}^{M-1}] \quad (73)$$

where SVD of  $\mathbf{H}_{c0}$  yields

$$\begin{aligned} \mathbf{H}_{c0} &\equiv \mathbf{U} \mathbf{\Sigma} \mathbf{V}^T \\ &\simeq [\mathbf{U}_R \ \mathbf{U}_D] \begin{bmatrix} \mathbf{\Sigma}_R & \mathbf{0} \\ \mathbf{0} & \mathbf{0} \end{bmatrix} \begin{bmatrix} \mathbf{V}_R^T \\ \mathbf{V}_D^T \end{bmatrix} \\ &= \mathbf{U}_R \mathbf{\Sigma}_R^{1/2} \mathbf{\Sigma}_R^{1/2} \mathbf{V}_R^T \end{aligned} \quad (74)$$

with  $R \equiv \text{rank}(\mathbf{H}_{c0})$ . Hence, the reduced-order model is given by

$$\mathbf{D}_0 = \text{the first } N_i \text{ columns of } \mathbf{Y}^0 \quad (75)$$

$$\mathbf{D}_1 = \text{the second } N_i \text{ columns of } \mathbf{Y}^0 \quad (76)$$

$$\mathbf{C} \simeq \mathbf{U}_R \mathbf{\Sigma}_R^{1/2} \quad (77)$$

$$\mathbf{B}_0 \simeq \text{the first } N_i \text{ columns of } \mathbf{\Sigma}_R^{-1/2} \mathbf{U}_R^T \mathbf{Y}^1 \quad (78)$$

$$\mathbf{B}_1 \simeq \text{the second } N_i \text{ columns of } \mathbf{\Sigma}_R^{-1/2} \mathbf{U}_R^T \mathbf{Y}^1 \quad (79)$$

$$\mathbf{A} \simeq \mathbf{\Sigma}_R^{-1/2} \mathbf{U}_R^T \mathbf{H}_{c1} \mathbf{V}_R \mathbf{\Sigma}_R^{-1/2} \quad (80)$$

## 7.2 Aerodynamic ROM with displacement inputs

The second scheme is to use only the displacements as the system inputs. This is possible by applying simultaneously the pulse and double pulse inputs,

$$u_i^n = \delta^n \equiv \begin{cases} 1 & (n = 0) \\ 0 & (n = 1, 2, \dots, M) \end{cases} \quad (81)$$

$$\dot{u}_i^n = \dot{\delta}^n \equiv \begin{cases} \frac{1}{\Delta\tau} & (n = 0) \\ -\frac{1}{\Delta\tau} & (n = 1) \\ 0 & (n = 2, 3, \dots, M) \end{cases} \quad (82)$$

and get the corresponding responses  $\mathbf{y}_{d1}^0, \mathbf{y}_{d1}^1$  at the first two time steps:

$$\mathbf{Y}_d^0 = [\mathbf{y}_{d1}^0 \ \mathbf{y}_{d2}^0 \ \dots \ \mathbf{y}_{dN_i}^0] \quad (83)$$

$$\mathbf{Y}_d^1 = [\mathbf{y}_{d1}^1 \ \mathbf{y}_{d2}^1 \ \dots \ \mathbf{y}_{dN_i}^1] \quad (84)$$

For a new SCI, we use

$$\mathbf{b}_{SCI}^n \equiv \sum_{i=1}^{N_i} \mathbf{b}_{0i} r_i^n + \sum_{i=1}^{N_i} \mathbf{b}_{1i} \dot{r}_i^n \quad (85)$$

$$\mathbf{d}_{SCI}^n \equiv \sum_{i=1}^{N_i} \mathbf{d}_{0i} r_i^n + \sum_{i=1}^{N_i} \mathbf{d}_{1i} \dot{r}_i^n \quad (86)$$

where  $\dot{r}_i^n$  are discrete-time derivative of  $r_i^n$ . To be consistent with the use of the double pulse defined in (82),  $\dot{r}_i^n$  are obtained by filtering  $r_i^n$  via  $\dot{\delta}_i^n$ , i.e.,

$$\dot{r}_i^n \equiv \text{conv}(r_i^k, \dot{\delta}_i^k) \quad (87)$$

which is equivalent to the backward difference equation,

$$\dot{r}_i^n \equiv \frac{r_i^n - r_i^{n-1}}{\Delta\tau} \quad (88)$$

Subject to the new SCI we sample the system response  $\mathbf{y}^n$  and get

$$\mathbf{y}_{dc0}^n \equiv \mathbf{y}^n - \sum_{i=1}^{N_i} \mathbf{y}_{di}^0 r_i^n \quad (89)$$

$$\mathbf{y}_{dc1}^n \equiv \mathbf{y}^{n+1} - \sum_{i=1}^{N_i} \mathbf{y}_{di}^0 r_i^{n+1} - \sum_{i=1}^{N_i} \mathbf{y}_{di}^1 r_i^n \quad (90)$$

Defining

$$\mathbf{H}_{dc0} \equiv [\mathbf{y}_{dc0}^1 \ \mathbf{y}_{dc0}^2 \ \dots \ \mathbf{y}_{dc0}^{M-1}] \quad (91)$$

$$\mathbf{H}_{dc1} \equiv [\mathbf{y}_{dc1}^1 \ \mathbf{y}_{dc1}^2 \ \dots \ \mathbf{y}_{dc1}^{M-1}] \quad (92)$$

the SVD of  $\mathbf{H}_{dc0}$  yields

$$\begin{aligned} \mathbf{H}_{dc0} &\equiv \mathbf{U} \mathbf{\Sigma} \mathbf{V}^T \\ &\simeq [\mathbf{U}_R \ \mathbf{U}_D] \begin{bmatrix} \mathbf{\Sigma}_R & \mathbf{0} \\ \mathbf{0} & \mathbf{0} \end{bmatrix} \begin{bmatrix} \mathbf{V}_R^T \\ \mathbf{V}_D^T \end{bmatrix} \\ &= \mathbf{U}_R \mathbf{\Sigma}_R^{1/2} \mathbf{\Sigma}_R^{1/2} \mathbf{V}_R^T \end{aligned} \quad (93)$$

with  $R \equiv \text{rank}(\mathbf{H}_{d_{c0}})$ . The new reduced-order model has only  $N_i$  input channels and is in the form

$$\mathbf{x}^{n+1} = \mathbf{A} \mathbf{x}^n + \mathbf{B} \mathbf{u}^n \quad (94)$$

$$\mathbf{y}^n = \mathbf{q} (\mathbf{C} \mathbf{x}^n + \mathbf{D} \mathbf{u}^n) \quad (95)$$

where

$$\mathbf{D} = \mathbf{Y}_d^0 \quad (96)$$

$$\mathbf{C} \simeq \mathbf{U}_R \Sigma_R^{1/2} \quad (97)$$

$$\mathbf{B} \simeq \Sigma_R^{-1/2} \mathbf{U}_R^T \mathbf{Y}_d^1 \quad (98)$$

$$\mathbf{A} \simeq \Sigma_R^{-1/2} \mathbf{U}_R^T \mathbf{H}_{d_{c1}} \mathbf{V}_R \Sigma_R^{-1/2} \quad (99)$$

### 7.3 Reduced-order aeroelastic model

We illustrate how aeroelastic systems can be constructed using the reduced-order aerodynamic models obtained in the previous section.

First, we note that structural model is normally described in real, continuous-time:

$$\mathbf{m} \ddot{\mathbf{u}} + \mathbf{c} \dot{\mathbf{u}} + \mathbf{k} \mathbf{u} = \mathbf{y} \quad (100)$$

( $\dot{\phantom{x}}$ ) and ( $\ddot{\phantom{x}}$ ), respectively, represent the first and the second derivatives with respect to  $t$ . Hence, to construct aeroelastic model the continuous-time equation (100) is discretized in time:

$$\mathbf{z}^{n+1} = \mathbf{A}_s \mathbf{z}^n + \mathbf{B}_s \mathbf{y}^n \quad (101)$$

$$\mathbf{u}^n = \mathbf{C}_s \mathbf{z}^n \quad (102)$$

where

$$\mathbf{z} \equiv \begin{Bmatrix} \mathbf{u} \\ \dot{\mathbf{u}} \end{Bmatrix} \quad (103)$$

$$\mathbf{C}_s \equiv [\mathbf{I} \quad \mathbf{0}] \quad (104)$$

Note that given  $\Delta\tau$  and  $V$  the consistent incremental time step,  $\Delta t = \frac{\Delta\tau b}{V}$ , must be used in the conversion to the discrete-time.

### Aeroelastic Model I.

In this approach, we treat  $\mathbf{u}^n, \dot{\mathbf{u}}^n$  as independent inputs and apply the  $\mathbf{b}_{SCI}^n, \mathbf{d}_{SCI}^n$  given by Eqs. (68) and (69) at a reference dynamic pressure,  $q_{ref} \equiv \frac{1}{2}\rho_{ref}V_{ref}^2$ . The corresponding samples are taken and scaled by  $\frac{1}{q_{ref}}$ . The ROM of the first kind described in Section 6.1 is then obtained by applying the SCI/ERA. An aeroelastic system that is valid at all  $V$  can be constructed by combining the resulting aerodynamic ROM with the structural equations:

$$\mathbf{X}^{n+1} = \mathbf{A}_{d1} \mathbf{X}^n \quad (105)$$

where

$$\mathbf{X} \equiv \begin{Bmatrix} \mathbf{x} \\ \mathbf{z} \end{Bmatrix} \quad (106)$$

$$\mathbf{A}_{d1} \equiv \begin{bmatrix} \mathbf{A} & [\mathbf{B}_0 & \mathbf{B}_1] \\ q\mathbf{B}_s\mathbf{C} & \mathbf{A}_s + q\mathbf{B}_s[\mathbf{D}_0 & \mathbf{D}_1] \end{bmatrix} \quad (107)$$

Denoting the eigenvalues of system matrix (107) as  $\lambda_{d1,i}$ , the aeroelastic eigenvalues in the Laplace domain are obtained as

$$\lambda_{c1,i} = \frac{\log(\lambda_{d1,i})}{\Delta t} \quad (108)$$

For flutter instability, one must have  $Real(\lambda_{c1,i}) > 0$  and  $||\lambda_{d1,i}|| > 1$  for any  $i$ .

### Aeroelastic Model II.

One can also apply the  $\mathbf{b}_{SCI}^n, \mathbf{d}_{SCI}^n$  given by Eqs. (85), (86) and get the ROM of the second kind described in Section 6.2. This will produce aerodynamic system matrices,  $\mathbf{A}, \mathbf{B}, \mathbf{C}$ , and  $\mathbf{D}$  where  $\mathbf{B}, \mathbf{D}$  each has only  $N_i$  columns. The new resulting reduced-order aeroelastic model can be obtained as

$$\mathbf{X}^{n+1} = \mathbf{A}_{d2} \mathbf{X}^n \quad (109)$$

where

$$\mathbf{A}_{d2} \equiv \begin{bmatrix} \mathbf{A} & \mathbf{B}\mathbf{C}_s \\ q\mathbf{B}_s\mathbf{C} & \mathbf{A}_s + q\mathbf{B}_s\mathbf{D}\mathbf{C}_s \end{bmatrix} \quad (110)$$

Although  $q$  can change in Eq. (110), this model must be used only at the reference air speed  $V_{ref}$ . It is well known that given a local angle of attack  $u$ , plunging rate  $\dot{u}$ , and local air speed  $V$  the total aerodynamic downwash at the moving boundary is  $\dot{u} + V u$  and as such it is impossible to separate out and account for the effect of  $V$  without having both the displacement and velocity channels. However, this drawback is easily remedied by adjusting the incremental time step according to  $\Delta t = \frac{\Delta \tau b}{V}$  when the air speed changes from one value to another and discretizing the structural model based on the new  $\Delta t$ . That is, if one leaves the  $V$  dependency in the structure,

$$\mathbf{A}_{d2} \equiv \begin{bmatrix} \mathbf{A} & \mathbf{B}\mathbf{C}_s \\ q\mathbf{B}_s(V)\mathbf{C} & \mathbf{A}_s(V) + q\mathbf{B}_s(V)\mathbf{D}\mathbf{C}_s \end{bmatrix} \quad (111)$$

then the Aeroelastic Model II. becomes valid for all air speeds.

## 8 Results and Discussion

### 8.1 Unsteady vortex lattice example

To demonstrate the proposed method, an unsteady vortex lattice aerodynamic model subjected to several structural mode inputs is considered. Both types of reduced-order aeroelastic models are constructed using the methods described in the previous section. For simplicity of implementation, only the results from the SCI/ERA method with a sufficient number of output measurements are presented here. Occasionally, the alternative scheme described in Section 4. was applied and indeed found to produce reduced-order models of essentially the same qualities as those presented here.

Unsteady flow field around a flat, rectangular wing in incompressible, subsonic air flow is modeled by the vortex lattice formulation (Figure 3). The wing is 3 inches wide and 12 inches long, has 10 and 20 vortex elements in the chordwise and spanwise directions, respectively. The free wake has 40 and 20 vortex elements in the stream-wise and spanwise directions, creating a total of 800 degrees of freedom[13]. The wing structure is modeled using 6 vibrational (3 bending and 3 torsional) modes[14].

No structural damping was introduced at this time. Thus, the size of the full-order aeroelastic model is  $(812 \times 812)$ .

For the Aeroelastic Model I. the reference air density and speed were set at  $1.23\text{kg}/\text{m}^3, 80\text{m}/\text{sec}$ , respectively. The incremental time at this reference speed is  $\Delta t = \frac{dx}{V_{ref}} = 9.525 \times 10^{-5}\text{sec}$ . For the sampling of the vortex model, 480 extra outputs were extracted in addition to the 6 generalized aerodynamic forces at 481 time steps. Applying 12 sets of random signal inputs simultaneously, 6 for  $\mathbf{u}^n$ , 6 for  $\dot{\mathbf{u}}^n$ , yielded a single set of sampled data. 12 pulse inputs were also applied individually at the first two time steps to generate  $\mathbf{Y}^0$  and  $\mathbf{Y}^1$ . Figure 4 shows three sets of the random numbers generated on Matlab. Out of 481 time samples, the SVD produced 413 linearly independent singular modes. This number was determined by the rank of  $\mathbf{H}_{c0}$  matrix. Thus, the size of the aerodynamic ROM became  $(413 \times 413)$ . The reduced-order aerodynamic model was then coupled with the structural model to create  $(425 \times 425)$  aeroelastic model (ROM I.).

For the Aeroelastic Model II. the reference air density and speed were again set at  $1.23\text{kg}/\text{m}^3$  and  $80\text{m}/\text{sec}$ . 6 sets of random signals and 6 sets of discrete-time derivatives of the random signals were applied for  $\mathbf{u}^n$  and  $\dot{\mathbf{u}}^n$  using 481 time steps and the 486 output measurements. This yielded  $(329 \times 329)$  aerodynamic ROM which when combined with the structural system, produced  $(341 \times 341)$  aeroelastic model (ROM II.). It is noted that ROM II. is approximately 20 % smaller than ROM I. as a result of using only the half of the input channels.

Next, the dimensions of the reduced-order aerodynamic models were further decreased using the FDKL/SCI method. As mentioned earlier, the incremental time step embedded in both the FOM and SCI/ERA ROM is too small to be effective for various aeroelastic simulations which usually involve a low frequency range. Considering that the highest free vibrational frequency of the structural modes is  $4,160\text{ rad}/\text{sec}$ , the sampling range in the FDKL method was restricted to  $(-4, 500, 4, 500)\text{rad}/\text{sec}$ . For the ROM I., out of 174 frequency samples within the range 129 KL modes were

selected based on the rank of the covariance matrix  $\mathbf{K}$ . Hence, the size of the new reduced-order aerodynamic and aeroelastic models (ROM I-FDKL) became 129 and 141, respectively. Likewise, for the ROM II. 97 KL modes out of 130 frequency samples in the same frequency range were selected yielding new  $(109 \times 109)$  aeroelastic model (ROM II-FDKL). For computational efficiency, these reduced-order models are to be preferred over the ROM I. and ROM II.

Figure 5 presents  $(6 \times 6)$  generalized aerodynamic forces obtained from the FOM, ROM I-FDKL, and ROM II-FDKL, in the nondimensional time,  $\tau$ . It is seen that despite the cut-off frequency range present in the latter two models, they reproduce the pulse aerodynamic responses of the original model very well.

Figure 6 and 7 show two different scales of the aeroelastic eigenvalues of the various models in the  $s$  domain at  $V = 80m/sec$ . It is seen that many eigenvalues of the reduced-order aeroelastic models match very well with those of the full model (Figure 6). More specifically, the 12 complex eigenvalues associated with 6 structural modes agree very well between the FOM and ROMs, although the higher structural modes (5th and 6th) in the ROM II. and ROM II-FDKL are slightly mismatched (Figure 7). Also noteworthy is that all the eigenvalues of the ROM I-FDKL and ROM II-FDKL are approximately within the specified bound,  $(-4, 500, 4, 500)rad/sec$  as the model was obtained based on frequency samples in the range. Presented in Figure 8 and 9 are time responses of the first two structural modes due to an initial condition in  $\dot{u}_1$ . It can be seen that the three sets of curves are practically indistinguishable from each other. Next set of figures, Figure 10-13 show aeroelastic results at  $V = 121.2m/sec$ . As can be seen from the figures, the wing is on the verge of flutter at this speed. Note how accurately the ROM I-FDKL is able to reproduce neutrally stable, sinusoidal time responses (Figs. 12-13). However, the ROM II-FDKL exhibits a noticeable but minor error in producing the transient response.

Finally, the model construction time is compared between the two ERA methods. In order to obtain accurate and consistent singular modes,  $\mathbf{H}_{c0}$ ,  $\mathbf{H}_{c1}$  matrices were

kept as square as possible by keeping the number of time samples approximately equal to the total number of measurements which is the sum of the number of generalized aerodynamic forces and the number of auxiliary measurements. The same numbers of time steps and auxiliary outputs were used both in the Pulse/ERA and SCI/ERA. Thus, in the first case where only the first bending mode alone excites the flow field,  $M = 131, N_o = 131$ . In the second case where the first bending and first torsional modes were included,  $M = 251, N_o = 252$ , and in the third case where the first bending and torsional as well as the second bending modes excite the aerodynamic field,  $M = 281, N_o = 283$ . 4 and 5 inputs were also used with  $M = 331, N_o = 334$  and  $M = 411, N_o = 415$ , respectively. Table 1. shows CPU seconds spent in constructing ROM I. on a SGI machine. Also presented in parenthesis are the dimensions of the corresponding reduced-order models. Table 2. shows CPU seconds consumed for ROM II. on the SGI machine. Presented again in Figure 14 is the CPU seconds vs. the number of inputs for ROM I. and ROM II. Note that these numbers represent total CPU seconds spent not only in sampling the response but also processing the data in the subsequent ERA schemes. As seen from the Tables and Figure, the new method clearly has an advantage over the Pulse/ERA in reducing the model construction time yielding saving factors of multiple numbers. Needless to say, as the number of inputs increases so does the saving. It is interesting that for a given number of inputs both ERA methods generate ROMs of very similar sizes. As expected, ROM II. of the SCI/ERA are as small as 80 % of the corresponding ROM I. Despite the different input channels, both SCI/ERA ROM I. and ROM II. require approximately the same CPU time implying that in the SCI/ERA the overall computation time is not very sensitive to the number of inputs.

## 8.2 CFL3D example

The SCI/ERA has also been applied to unsteady aerodynamic systems modeled by CFL3D code. CFL3D is a finite element program that based on the Navier-Stokes

equations models nonlinear viscous, compressible fluid motion in subsonic as well as transonic flow fields[15]. Although CFL3D describes statically and dynamically nonlinear flow, when subjected to a small amplitude it predicts dynamically linearized behavior of the flow field around the nonlinear static position in the form of Eqs. (58) and (59). For most practical aeroelastic analyses such as flutter prediction and dynamic gust loads calculation, the small amplitude approximation yields sufficiently accurate results.

The aeroelastic formulation for the CFD code is slightly different than for the vortex lattice case in that the second aerodynamic model in section 6.2 is used but whenever the air speed  $V$  is changed the incremental time step  $\Delta t$  is adjusted accordingly when discretizing the structural model, Eq. (100). As in the Aeroelastic Model I. the resulting model can account for the effect of changing the free stream speed. The airplane configuration under consideration is that of the Twin-Engine-Transport-Flutter-Model (TETFM). The aerodynamic grid is given by the so called the Wing-Pencil-Nacelle (WPN) model with the strut between the wing and nacelle omitted (Figure 15). The structural motion is described by 10 structural modes, resulting in total of 10 generalized aerodynamic forces per a mode shape. Figure 16 shows the first 4 mode shapes. The computational aerodynamic model consists of approximately 700,000 cells and 30 blocks. For detailed description of the modeling, see Ref.[3]. Ref.[12] discusses the computational model and construction of the aerodynamic and aeroelastic ROMs based on the SCI/ERA using various types of input signals mentioned earlier. In this section, only one set of ROM results that were obtained from the SSCI/ERA are presented from the cited reference.

The WPN model was examined at  $M = .831$ . With  $\Delta t = 3.34 \times 10^{-4} \text{sec}$  and 995 time steps, aerodynamic ROMs were created using both the Pulse/ERA and SSCI/ERA methods based on the displacement method described in section 6.2. The size of the aerodynamic ROMs is  $(512 \times 512)$ . Given the 10 mode inputs, the total number of time steps consumed in the time marching required for the SCI/ERA

process was  $995 + 81 \times 10 = 1805$ . On the other hand, the traditional ERA required total of  $10 \times 995 = 9,950$ . Using a single CPU of IBM/Regatta machine, the total CPU hours for the Pulse/ERA calculation was 366 while the SSCI/ERA required only 64 hours. Thus, the computational cost was reduced by a factor of 5.7. Figure 17 shows the V-g plot of the two different aeroelastic models. As seen from the figure, the two ROMs match very well in flutter characteristics predicting the two flutter points within just 0.13 % and 0.36 % differences, respectively.

## 9 Concluding Remarks

In this paper, an efficient time-domain model reduction/system identification technique has been presented and demonstrated for linear dynamic systems that are subjected to multiple right-hand-side inputs. The method is 100 % a post-processing that does not require modifying the original code and takes only input and output data for the model construction. The new method is based on a direct singular value decomposition of the output measurements that are not necessarily attributed to pulse inputs but due to multiple signal inputs applied simultaneously at the input channels. Compared to the Pulse/ERA, the SCI/ERA can significantly reduce the model construction time and compress the amount of output data. Therefore, it is very attractive for large-scaled dynamic systems with multiple driving inputs such as CFD models wherein the moving boundary input is often described by many structural modes. For practical applications a second model reduction of the ERA ROM is desirable. For this purpose, the FDKL/SCI method is recommended for its efficiency and accuracy.

## Acknowledgment

The author is grateful to his manager, Steven R. Precup and Senior Technical Fellow, Kumar G. Bhatia for their continuous support for this research. Note that the algorithm presented in this paper is a Boeing Intellectual Property under consideration

Table 1: CPUs of ERAs Applied to VLM (ROM I.)

$N_i$	Pulse/ERA	SCI/ERA
1	12.3 <i>sec</i> (92)	6.7 <i>sec</i> (89)
2	74.8 <i>sec</i> (180)	16.6 <i>sec</i> (182)
3	150.8 <i>sec</i> (221)	20.6 <i>sec</i> (226)
4	327.8 <i>sec</i> (297)	28.2 <i>sec</i> (298)
5	762.3 <i>sec</i> (336)	43.7 <i>sec</i> (340)
6	1,525.5 <i>sec</i> (395)	63.2 <i>sec</i> (413)

NOTE: Number in ( ) is the size of ROM.

Table 2: CPUs of ERAs Applied to VLM (ROM II.)

$N_i$	Pulse/ERA	SCI/ERA
1	6.3 <i>sec</i> (92)	6.8 <i>sec</i> (89)
2	32.8 <i>sec</i> (169)	17.00 <i>sec</i> (167)
3	65.9 <i>sec</i> (215)	21.0 <i>sec</i> (214)
4	130.1 <i>sec</i> (258)	27.6 <i>sec</i> (257)
5	279.6 <i>sec</i> (304)	44.1 <i>sec</i> (305)
6	540.4 <i>sec</i> (316)	61.4 <i>sec</i> (329)

NOTE: Number in ( ) is the size of ROM.

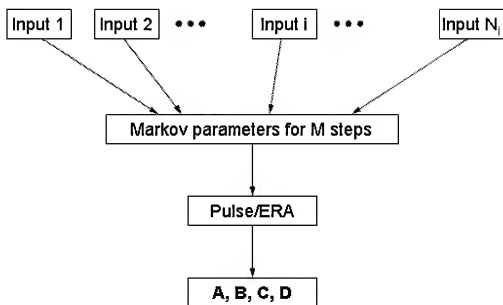


Figure 1: Schematic of Pulse/ERA process.

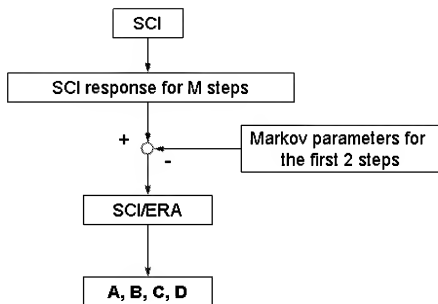


Figure 2: Schematic of SCI/ERA process.

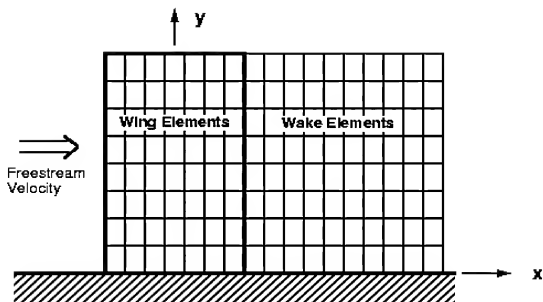


Figure 3: Vortex lattice grids for rectangular semi-span.

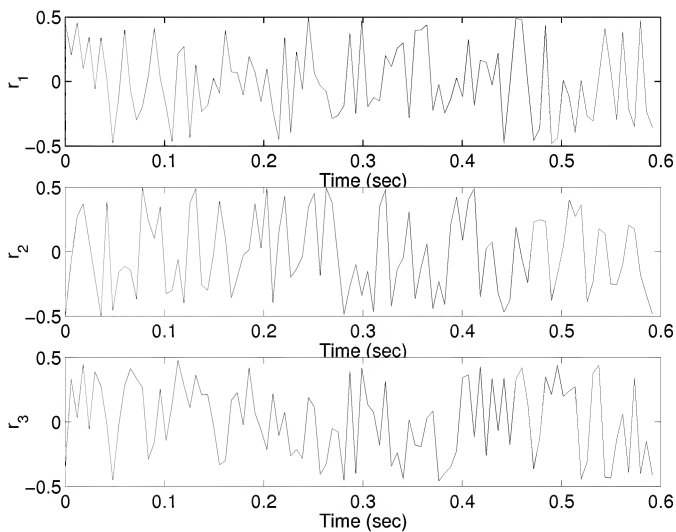


Figure 4: Statistically independent random signals.

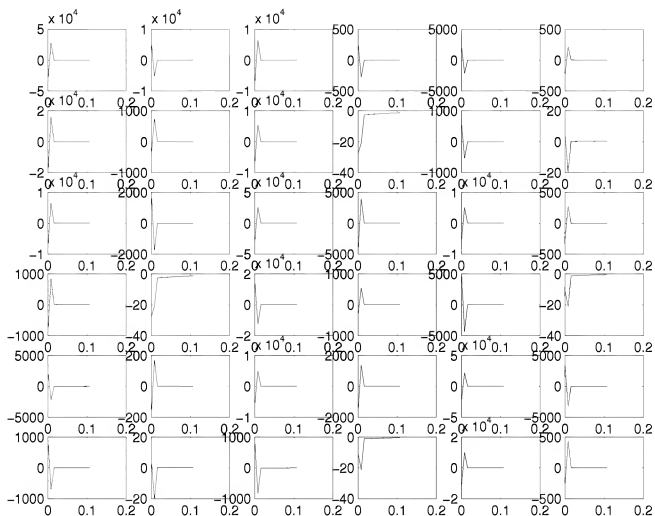
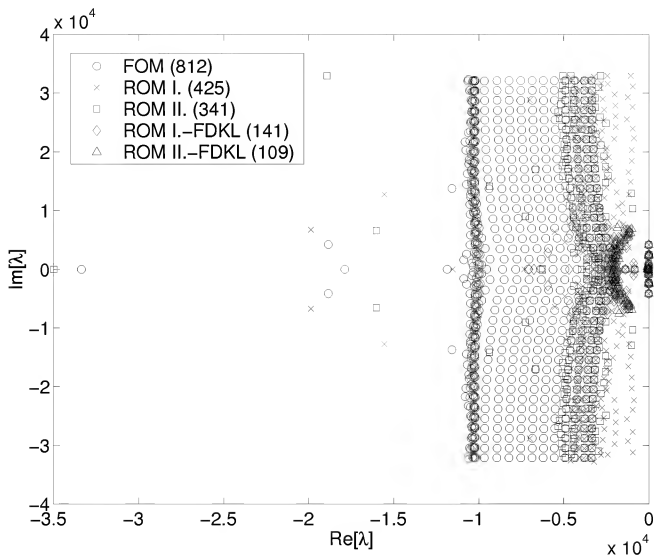
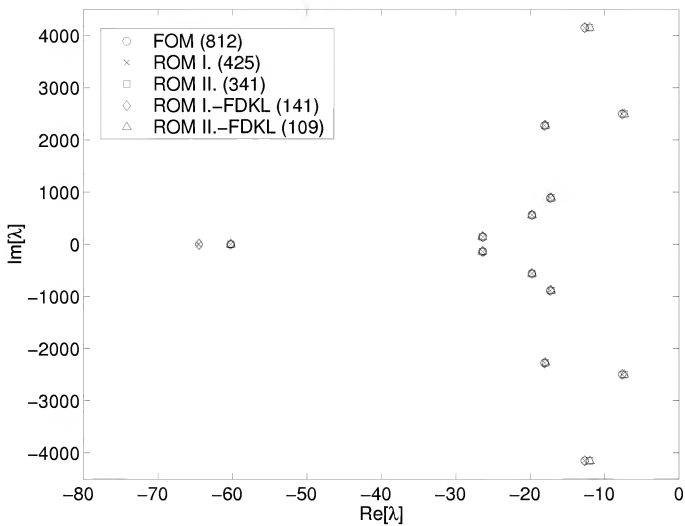


Figure 5: Generalized aerodynamic forces at  $V = 80m/sec$  ( - FOM (800) - - ROM I-FDKL (129) ... ROM II-FDKL (97)).

Figure 6: Aeroelastic eigenvalues at  $V = 80 \text{ m/sec}$ .

Figure 7: Aeroelastic eigenvalues at  $V = 80 \text{ m/sec}$ .

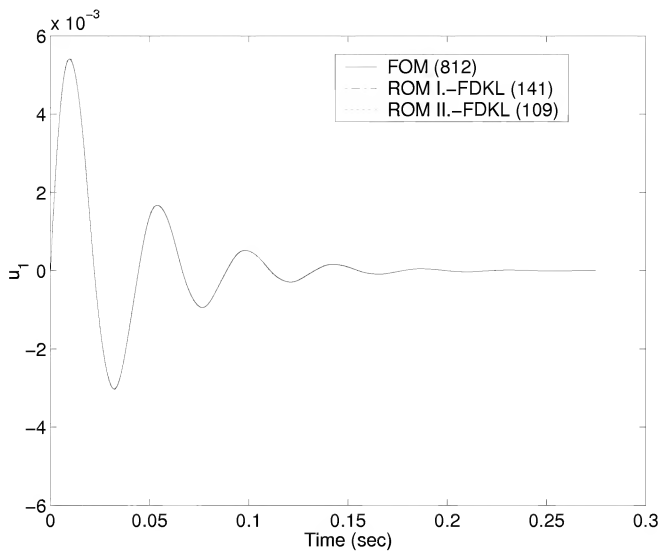


Figure 8: Mode 1 aeroelastic response due to IC in mode 1 at  $V = 80 \text{ m/sec}$ .

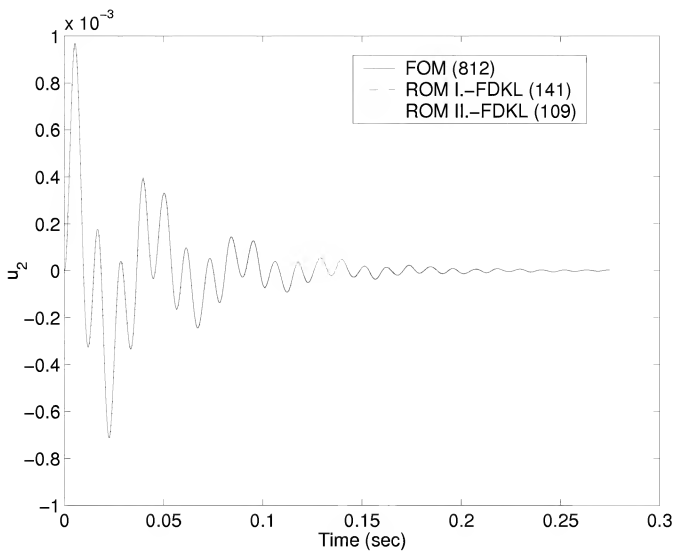
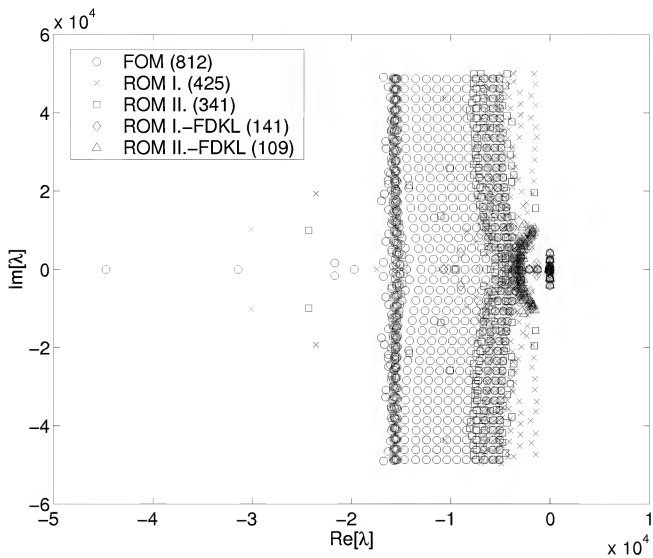
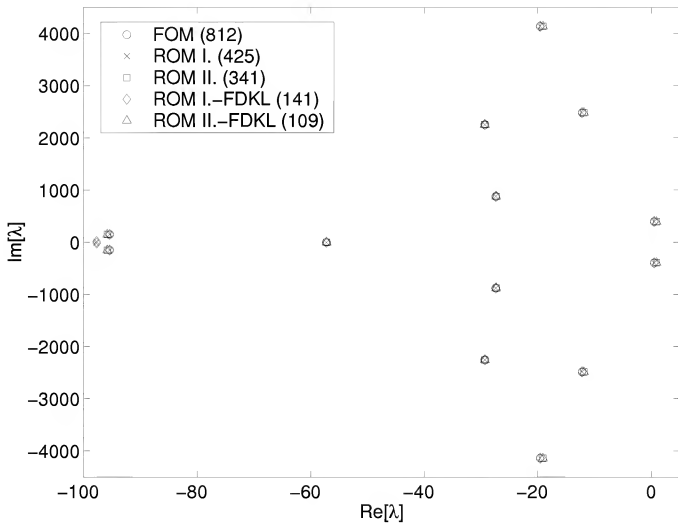


Figure 9: Mode 2 aeroelastic response due to IC in mode 1 at  $V = 80 \text{ m/sec}$ .

Figure 10: Aeroelastic eigenvalues at  $V = 121.2 \text{ m/sec}$ .

Figure 11: Aeroelastic eigenvalues at  $V = 121.2 \text{ m/sec}$ .

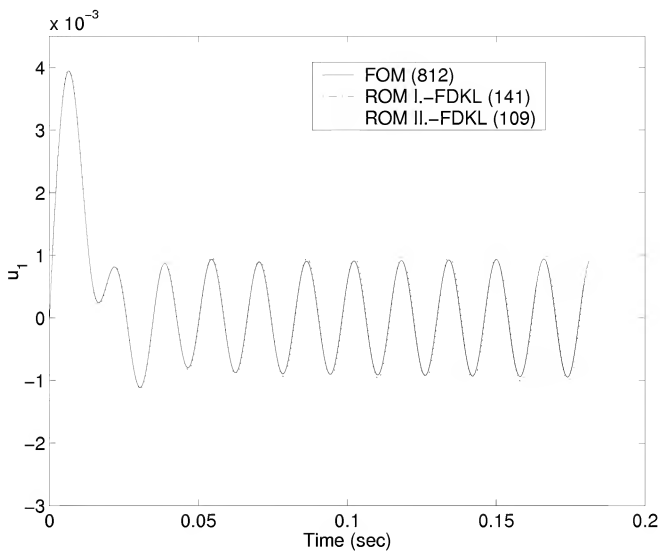


Figure 12: Mode 1 aeroelastic response due to IC in mode 1 at  $V = 121.2 \text{ m/sec}$ .

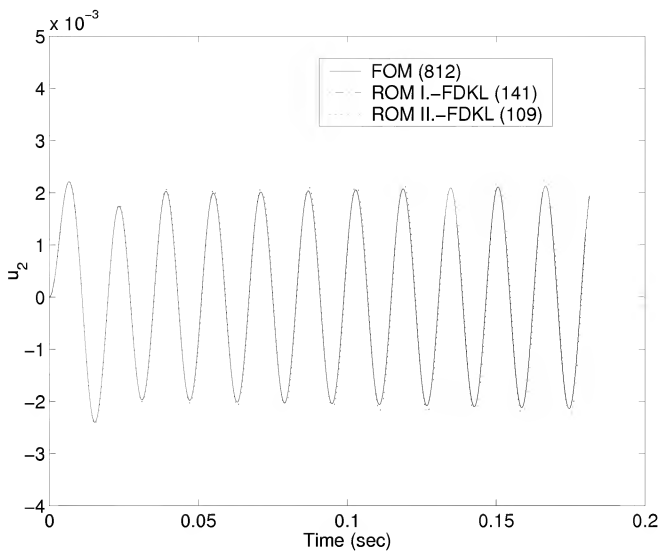


Figure 13: Mode 2 aeroelastic response due to IC in mode 1 at  $V = 121.2m/sec$ .

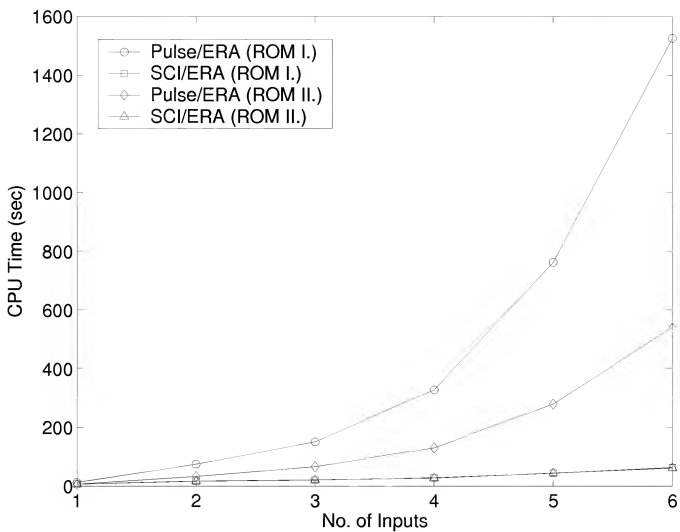


Figure 14: Model construction time of VLM ERA ROMs vs no. of inputs.

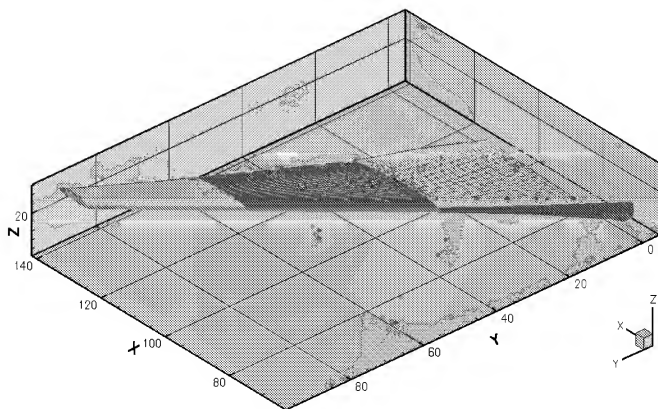


Figure 15: The CFL3D grids for WPN model.

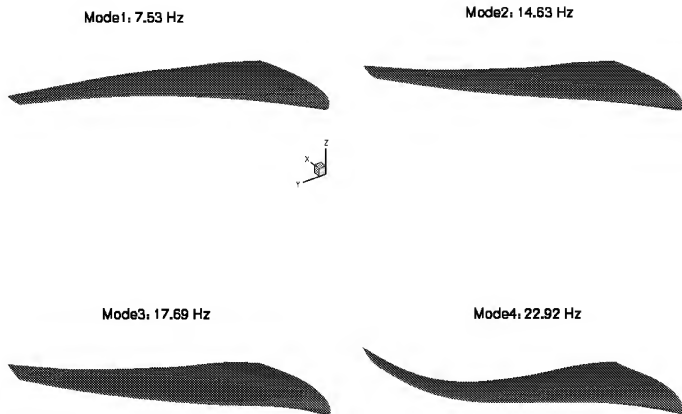


Figure 16: First 4 structural mode shapes for WPN model.

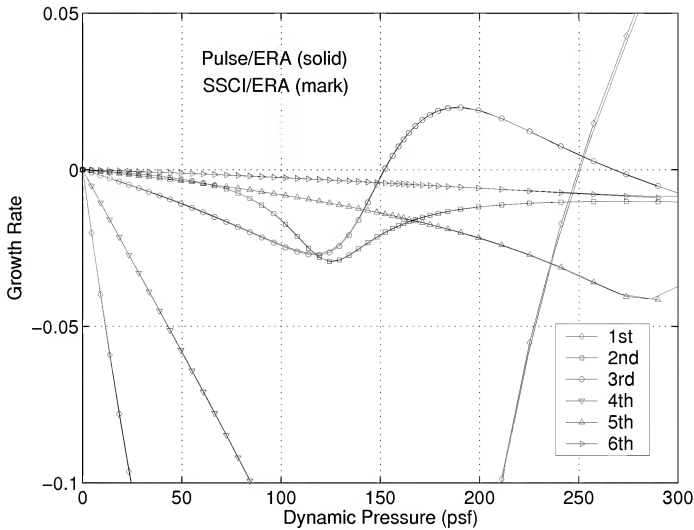


Figure 17: V-g plot of WPN model: Pulse/ERA vs. SSCI/ERA (growth rate only).